Design, synthesis, characterization, catalytic, fluorometric sensing, antimicrobial and antioxidant activities of Schiff base ligand capped AgNPs

G. Suneetha
University College of Science, Osmania University
P. Sunitha Manjari (psmanjari76@gmail.com)
University College of Science, Osmania University

Research Article

Keywords: Schiff base ligand, Ag NPs, Surface plasmon resonance, Catalytic degradation, Fe2+ detection, Biological activities

Posted Date: June 23rd, 2022

DOI: https://doi.org/10.21203/rs.3.rs-1744721/v1

Abstract

In recent days, the usage of biological and non-biological pollutants increases and it poses a significant threat to environmental and biological systems. Therefore, the present aim is to develop effective methods to treat such pollutants by using highly stable and small-sized Schiff base ligand capped silver nanoparticles (AgNPs) with a face-centered cubic (fcc) crystalline structure and the size range is 5–10 nm. The potent role of the resulting synthesized AgNPs was found as multiple platforms such as catalyst, sensor, antioxidant, and antimicrobial disinfectant. The synthesized AgNPs were characterized through UV–vis spectroscopy, PL, FTIR, XRD, SEM, and TEM. The FTIR spectrum of AgNPs exhibited the interacted functional groups of Schiff base and size was estimated by XRD and TEM. AgNPs were able to catalytically degrade approximately 95% of methylene blue (MB), rhodamine B (RhB), and eosin Y (EY) dyes within 80 min of reaction time using NaBH4. The fluorometric sensor studies of synthesized AgNPs showed selective sensing of the potentially hazardous Fe^{2+} ion in water. As an antimicrobial agent, the AgNPs are effective against both Gram-positive and Gram-negative bacteria; as well as fungi, with the zones of clearance as approximately compatible with standard drugs. The AgNPs displayed a greater ability to scavenge free radicals, especially DPPH when compared with AgNPs and ascorbic acid. Thus, the results of this study validate the triple role of AgNPs derived via a simple synthesis as a catalyst, sensor, antioxidant, and antimicrobial agent for effective environmental remediation.

1. Introduction

In general, Schiff bases can be prepared by facile condensation of carbonyl with primary amines or substituted primary amines with different reaction conditions [1–6]. Among them, bidentate salicylaldehyde derived Schiff base compounds have received much attention fortheir versatile and flexible properties to form transition metalcomplexes [1–6]. Most of the transition metal complexes coordinated with Schiff baseshas played an important role in coordinationchemistry for their interesting their structure, applications, andproperties [7–8]. Although during the recent years, considerable attention has been paid to the thermal behaviour oftransition metal complexes containing Schiff base substituted salicylaldehyde derivatives, which is one ofthe important properties of complexes indicating thermalstability and decomposition process under various conditions [9–10], however much less has been studied withcorresponding N,O-bidentate ones [11]. Schiff bases coordinated metal complexes have found applications in catalytic reactions [12] and as models for biological systems [13]. In addition, the nano forms of the Schiff bases and its derived metal complexes are desirable to develop in the fields of catalytic and biological applications. On the other hand are among the least areas of research in nanoscience that may hold great pharmaceutical applications.

In the development of nanotechnology, the nanoparticles play an important role in various research fields such as catalytic, sensing and biological applications [14] due to its higher surface area and stability [15]. In the biological field of applications, nanoparticles are enrich in the biological activity than other than nanoparticles because of its bio-compatibility especially in biological field [14], but the synthesizing nanoparticles is more complicated [16] because, the reactivity of the stabilizing or capping agents with

metal precursors is very low [17]. In some cases the size of the stabilized or capped nanoparticles is increased by the influence of atmospheric parameters [18]. These problems decrease the attention of researchers in the synthesizing of bio-active nanoparticles. These bio-active nanoparticles were developed by number of techniques [19–21] and the synthetic way is very difficult and unclear. Therefore, we have chosen the best one of the easiest method, that is Brust-Schiffrin technique [22] which is carried out by two step phase transfer assisted synthesis for the synthesis of nanoparticles. It involves reduction of metal ions, stabilization and transfer of stabilized metal nanoparticles from aqueous to organic phase. The reactivity of stabilizing ligand and their solubility in organic solvents play critical role insynthesizing organic ligand stabilized metal nanoparticles [23]. Organic ligands like amines, thiols, imine, amide and hydroxyl compounds are used to stabilize or cape the metal nanoparticles [24–26]. Among the capping ligands, Schiff base has high reactivity and stabilizing ability with metal precursors and also it has more biological activities [27]. So my present study focused to synthesis a biologically active Schiff-base ligand capped AgNPs.

From the decades, metal nanoparticles are gaining more attention in the field of nanotechnology due to the higher specificity and activity than their bulk counterpart [28]. Metal NPs such as silver, gold, palladium, and platinum NPs have been broadly used as photonics, electronics, optical device, catalyst, sensing and bio-labelling agents. Among the metal NPs, AgNPs have found appropriate claimants as antimicrobial and anticancer agents; wound healing, drug delivery system and waste water treatment [29–30].Nowadays, harmful chemical substances such as organic dyes have become the root cause of water contamination. So, the catalytic degradation of organic dyes using synthesized AgNPs received the attention of scientists due to the high potential of degrading organic dyes.Other important properties of AgNPs, such as sensing and antimicrobial properties have been addressed previously [31].

Recently, several research groups have been synthesized nanoparticles via thermal decomposition method of Schiff base complexes [32–33]. However, various precursors have been used for the preparation of metal NPs via different methods [34–35], but there is no report on the Schiff base as a capping agent. Herein, we report the synthesis, characterization, and catalytic, sensing, and biological studies of AgNPs with capping of Schiff base (2-[(4-methoxy-phenylimino)-methyl]-4-nitrophenol). The synthesized AgNPs were also characterized using TEM, SEM, XRD, PL, UV-vis absorption, and FT-IR. Further, the synthesized AgNPs have also been used as catalyst for the degradation of MB, RhB, and EY dyes using $NaBH_4$ as a reducing agent.The antimicrobial activity of AgNPs was investigated against several bacteria and fungi. The fluorometric sensor studies of AgNPs showed selective sensing of the potentially hazardous Fe^{2+} ion in water.

2. Experimental

2.1. Materials and Methods

All the chemicals were purchased and received analytical grade. $AgNO_3$, $NaBH_4$, p-Anisidine, nitrosalicylaldehyde, methanol, acetone, andchloroform have been purchased from Merck and used as

received. For sensing activity, $Pb(NO_3)_2$, $CoCl_2.6H_2O$, $FeSO_4$, KCl, $MgSO_4$, $NiSO_4.6H_2O$, Hg_2Cl_2, $Sr(NO_3)_2$, $CaCl_2$, $BaCl_2$, $Al(NO_3)_3.9H_2O$, $Cr(NO_3)_3.9H_2O$ and $CdCl_2$were all purchased from Merck Chemical Reagent Co., Ltd. (India). Methylene blue, rhodamine B, and eosin Y have been purchased from Merck and used asreceived.Sterilized deionized water was used during the whole experiment process.

2.2. Synthesis of 2-[(4-methoxy-phenyl)iminomethyl]-4-nitrophenol (Schiff Base)

In the typical process for the synthesis of Schiff-base, i.e., 2-[(4-methoxy-phenyl)iminomethyl]-4-nitrophenol, ($C_{14}H_{12}N_2O_4$) was synthesized by using p-anisidine in methanol and this was slowly added to 5-nitrosalicylaldehyde in methanol as shown in Scheme 1. The mixture was refluxed and stirred for 3 hours at room temperature. The completion of the reaction was monitored through TLC for the disappearance of the starting compounds. Then, the solvent was evaporated yielding yellow precipitation of 2-[(4-methoxy-phenylimino)-methyl]-4-nitrophenol. The yield was about 85%. The solid thus obtained was dried in oven at 60 ^oC for 1 hour.

Analytical data of Schiff base

Colour: Yellow,

Yield: 85%,

M.P.: 162^oC.

FTIR (υ, cm^{-1}): 3618 (υ-O-H), 3072 (υ-C-H), 1621 (υ-C = N), 1516 (υ-C = C), 1336 (υ-N-O), 1258 (υ-C-O), 887 (υ-C-N).

UV (λ_{max}/nm): 236, 352.

^{1}H-NMR ($CDCl_3$, δ, ppm): 14.8 s 1H, 8.7 s 1H, 8.2–8.4 d 2H, 7.2–7.4 d 2H, 6.9–7.1 m 3H, 3.9 s 3H.

ESI-MS: m/z = 273.2 (M + 1).

2.3. Synthesis of Schiff base capped AgNPs

In a typical process for the synthesis of AgNPs were synthesized by Brust-Schiffrin technique, which is a two-step phase transfer synthesis as reported in the previous work [36]. In during the process, equal molar ratio of $AgNO_3$ and sodium borohydride ($NaBH_4$) was dissolved separately in ethanol and triple distilled water respectively. Both solutions were purged with nitrogen for 30 min and then the $NaBH_4$ solution was slowly added drop-wise to the ethanolic solutions of $AgNO_3$ with vigorous stirring and the temperature was maintained above 60°C in nitrogen atmosphere. After the addition completed, synthesized Schiff base ligand was dissolved in acetone and introduced to the aqueous solutions and vigorously stirred for five hours. After the completion of reaction the organic layer color changes from yellow to dark brown

and black indicates the formation of Schiff base capped AgNPs. The organic layer was carefully separated and washed with triple distilled water four times and reduced to 20% in rota evaporator. This reduced organic phase solutions was stored overnight and di-ethyl-ether was added and dark solid precipitate obtained was isolated and washed with petroleum ether for several times and recrystallized by ethanol. The schematic representation for the synthesis of Schiff base capped AgNPs is shown in Scheme 2.

2.4. Characterizations

The absorption spectra of the synthesized Schiff base and its AgNPs were measured on a UV-3600 UV–vis spectrophotometer. Photoluminescence spectrum was recorded on RF-5301 PC spectrophotometer with the excitation wavelength is 310 nm. FTIR spectroscopy (Bruker, US) was used to analyze functional groups which are involved in reduction of $AgNO_3$ into AgNPs with the transmittance was recorded at 500 to 4000 cm^{-1}. XRD (X-ray diffractometer, X'pert Pro, Japan) was used to obtain diffraction pattern of AgNPs with Cu Kα radiation (λ = 1.54 Å) between 20° to 70° (2θ range). Morphological features were studied by using Hitachi-7000 scanning electron microscope (SEM). TEM analysis was done by ultrasonically dispersal of AgNPs powder in ethanol. Further, the one drop of the dissolved sample was placed on a Cu grid and allowed to evaporate at room temperature and operating at 200 kV with a resolution point of 2.04 nm.

2.5. Catalytic degradation of dyes

In the part of the catalytic degradation of different dyes including MB, RhB and EY, three different set of reactions were performed to estimate the catalytic potential and percentages of degradation using the synthesized AgNPs in the presence of $NaBH_4$. Before degradation process the synthesized AgNPs were sonicated using ultra-probe sonication for few minutes to make aqueous colloidal suspension in dark. For degradation, colloidal suspension of 1 mg/mL of AgNPs and $NaBH_4$ was mixed with aqueous solution of dyes separately. The concentrationsof dyes were prepared from stock solution to 2×10^{-5} M. All three sets of reactions were observed for 80 min. The rate of dye degradation was monitored by taking 2 mL samples from each set every 10 min, and recording the UV–vis spectra. As a control experiment, only dye solutions were degraded without catalyst and compared with the other set of reactions in the presence of catalyst.The complete degradation reactions were followed pseudo-first-order rate kinetics and it was analyzed to evaluate the rate constant as per following equation:

$$\ln(A_t/A_0) = -kt$$

The % degradation of the dyes was estimated through the following equation:

$$\text{Percentage of degradation (\%)} = A_0 - A_t / A_0 \times 100$$

where, A_0 is the initial absorbance of dye, A_t is the absorbance of dye at time t and k is the rate constant. The whole reaction of degradation was processed at room temperature.

2.6. Fluorometric detection

In a typical procedure of detection of heavy metal ions including alkali and alkaline earth metal ions was performed according to the previously reported procedure with slight modifications [37]. An amount of 100 µL 0.1 µM metal ion solutions, such as Pb^{2+}, Cd^{2+}, Co^{2+}, Fe^{2+}, K^{+}, Mg^{2+}, Hg^{2+}, Ni^{2+}, Sr^{2+}, Ca^{2+}, Ba^{2+}, Al^{3+} and Cr^{3+} were respectively added into 1.84 mL pH 4.0 PBS solution, followed by adding 20 µL of the synthesized AgNPs, 20 µL 0.01 M TMB and 20 µL 10 M H_2O_2. After incubating for 20 min, the resulting solution was transferred to a quartz cuvette, characterized by recording the spectrofluorometer over the wavelength ranging from 300 to 700 nm with an excitation wavelength is 310 nm. For the selective detection of Fe^{2+} among other metal ions, an amount of 100 µL different concentrations of Fe^{2+} (0.1 µM to 100µM) were added into 100 µL pH 4.0 PBS and the synthesized AgNPs solutions. The mixtures were transferred to a quartz cuvette, characterized by recording the PL spectra. Then, the emission spectra were obtained during 10 min, and color changes were observed by the naked eye.

2.7. Antimicrobial activity test

The synthesized AgNPs were tried for antimicrobial action by agar well diffusion technique against the following microorganism, i.e., *Pseudomonas aeruginosa*, *Escherichia coli*, *Staphylococcus aureus* and *Bacillus subtilis* as Gram-positive and Gram-negative bacteria; *Aspergillus niger* and *Candida albicans* as fungi. The formation of clearing zones was measured in mm using the ruler scale method and compared with standard *ampicillin* and *ketoconazole* (positive control for bacterial and fungal activity, respectively). In brief procedure, 100 µL of a log phase cultures were seeded in the nutrient agar medium (beef extract, peptone and agar) for bacteria's. After solidification of all agars Petri plates 8 mm diameter five wells were formed by punching with sterile borer. In four wells 100 µL of various concentrations of AgNPs samples (0.2, 0.4, 0.6, and 0.8 µg/mL) and in one well *ampicillin* with equal concentration as positive control were loaded. At 37°C in incubator the petri plates were incubated for 24 h. The experiment was performed in triplicate for each pathogenic bacterium's and compared with the standard. Zone of inhibitions was measured by means of ruler method.

The antifungal activities of the synthesized Schiff base ligand and AgNPs were measured by agar dilution method [38] and inhibition percentage against the mycelia growthdiameter was expressed. The fungal strains for experimentincluding *A. niger* and *C. albicans* were separated from their different host plants. These pathogenswere further purified in water agar medium with hyphaltip and single spore methods. Before the experiment, they werecultured for 4 days at 25°C on potato dextrose agar (PDA). Each diluted solution (1 mL) was mixed with PDA (10 mL) and then put in the petri dish. Finally, the spores from amycelia disk (5 mm in diameter) were put on the middle part of the PDA plate. All plates were put into an incubator (25°C) until fungal colony in the control petri dish (DMSO) cover the whole surface of the petri dish. This experimentwas replicated four times in a thoroughly random model. The zone of inhibitions were measured and compared with the positive control.

2.8. Antioxidant activity test

The antioxidant activity of the synthesized AgNPs was measured by 2,2-diphenyl-1-picrylhydrazyl (DPPH) radical scavenging assay [39]. 4 mg of DPPH was dissolved in 100 mL of methanol and stored at 20°C. From the stock solution, 2 mL of solution was added to 1 mL methanol solution containing test samples of Schiff base and AgNPs at optimal concentration of 100 µg/mL. The DPPH free radical scavenging activity (RSA) was measured at 517 nm and standard compound is ascorbic acid. The percentage of free radical scavenging activity was calculated by using the following equation:

RSA (%) = (Control absorbance - Sample absorbance) / Control absorbance) × 100

3. Results And Discussion

3.1. Analysis of the synthesized Ag NPs

UV-visible absorption

The electronic bands of UV-vis absorption spectra of Schiff base and AgNPs were recorded in the range of 200–800 nm. The exhibited absorption bands were assigned to intraligand charge transition (ILCT)bands and shown in Fig. 1. For Schiff base, the maximum absorption band at 356 nmwas assigned to π→π* transition of N = N linkage andaromatic rings. Also, the n→π* electronic transition was observed at 422 nm, it is attributed to the azo aromaticchromophore and intra-molecular charge transfer interaction[40]. In the UV-vis absorption spectra of AgNPs, the maximum absorption band was observed at 438 nm (Fig. 1). In this case, the blueshift was found and absorption bands shifted to a lowerwavelength, probably due to the effect of the sizequantization. The decrease in particle size creates a blue shift [41]. The appearance of surface plasma resonance (SPR) band at 438 nm for AgNPs specifies the formation of nanoparticles [42]. Free Schiff base ligand peak at 264 nm shifted to higher wavelength also confirms that the Schiff base strongly interacted with the AgNPs.

Photoluminescence spectra

The photoluminescence of noble metal NPs could be viewed as an excitation of electrons from occupied *d*-bands into states above the fermi level. Subsequent electron–phonon and hole-phonon scattering processes led to energy loss and finally photoluminescent recombination of an electron from an occupied *sp*-band with the hole. Figure 2 shows that the PL spectra of Schiff base and AgNPs recorded at room temperature. It shows that excitation spectrum of AgNPs, which has shown the strong excitation peak at 390 nm with the emission wavelength 484 nm, and Schiff base shown as strong emission peak at 528 nm. PL spectra of Schiff base and AgNPs (Fig. 2) indicate that fluorescence of AgNPs is suppressed compared to Schiff base by a combination of inorganic nanoparticles with the organic ligands [43]. Since photoexcited electrons are transferred from the conduction band of AgNPs to the lowest unoccupied molecular orbital of Schiff base ligand (LUMO), it can modulate the emission behaviour of AgNPs.

FTIR spectra

FTIR spectra were recorded of Schiff base and Ag NPs between the wavenumber spanning over a range of 4000–400 cm^{-1} for the involving functional groups in the preparation of AgNPs as shown in Fig. 3. In the IR spectrum of Schiff base ligand, the azomethine nitrogen (-CH = N-) peak appeared at1621 cm^{-1} [44]. This frequency is shifted towards lower frequency at 1571 cm^{-1} for AgNPs which shows that azomethine nitrogen was stabilized the metal nanoparticles. A broad peak at3618 cm^{-1} in free ligand which does not disappeared in the FTIR spectrum of AgNPs. This result shows that phenolic oxygen atomnot involved in the stabilization of AgNPs. The other prominent IR peaks of Schiff base ligand and AgNPs were 3442.75, 3072.97, 1732.13, 1621.97, 1516.21, 1400.37, 1316.49, 1078.24, 887.14, 800.49 and 611.45 cm^{-1} which correspond to –O-H, -C = O, -C-N, -N = O, -C-H, -C-C, and –C = C bands in alcohol or phenol, amines, aromatics, aromatic amines, aliphatic amines, aromatics, nitro compounds, and alkenes presented in the Schiff base. However, the common trend in terms of prominent IR peaks, 3436.24 cm^{-1} and 1621.97 cm^{-1} were indicates the presence of –O-H and –N = O groups are actively involved in the reduction of Ag^{+} to Ag^{0}.

Powder XRD

The determination of crystalline nature and structure of the synthesized AgNPs were by using XRD crystallography technique. The XRD pattern of the synthesized Schiff base and its stabilize AgNPs showed the Bragg's reflection plane in the 2θ range between 20–70°. In the XRD pattern of AgNPs, the diffraction peaks at 2θ = 38.21°, 44.39°, and 64.49° are corresponded to (111), (200), and (220) Miller indices of AgNPs and it was shown in Fig. 4, which interpreted for the face-centred cubic structure of the AgNPs [45]. The broad peaks presented in the XRD pattern indicated that the small crystalline sized nanoparticles were presented in AgNPs. The obtained other peaks illustrate that silver ions had indeed been reduced to Ag by the ligand under reaction conditions.The resulted XRD patter Bragg's diffraction peaks of AgNPs are well matched and corroborated with database of Joint Committee on Powder Diffraction Standard of AgNPs (JCPDS card No. 04–0783) [46]. The sharp peaks are shown in Fig. 4 might have due to capping agent which stabilize the AgNPs and few unassigned peaks that might be thought due to the crystallization of the Schiff base on the surface of the AgNPs. The lattice constant was calculated from diffraction pattern α = 4.11 Å and d-spacing 2.14 Å of synthesized AgNPs. The synthesized AgNPs crystalline size was calculated using Scherer's formula:

$$D = 0.9 \lambda / \beta \cos \theta$$

Where, D is the crystalline size, β is the full width at half maximum, λ is the wavelength of X-ray used (1.5406 Å) and θ is the Bragg's angle. The crystallite size was calculated to be approximately 10 ± 2 nm, which is in good agreement with the TEM results.

SEM and TEM

In detail estimation of structure, morphology and size of the synthesized AgNPs were observed from SEM and TEM images and it was shown in Fig. 5. The SEM images of Schiff base shows as needles type

structures and Schiff base ligand capped AgNPs were clearly shows that the surface of the AgNPs is uniform and spherical in shape.TEM also clearly shown as synthesized AgNPs have spherical shape with smooth surface and well dispersed. The small dots in the white barebackground were dispersed nanoparticles. It clearly confirms that the synthesized AgNPs are nano in size. The resultant AgNPs completely revealed that the Schiff base can protect Ag nanoparticles from aggregation efficiently. The broad TEM (Fig. 6) was developed by considering AgNPs; it clearly recommends that the mean size dispersion of AgNPs is 10 ± 2 nm. It exhibits the distribution of AgNPs inside ligand matrix that might be attributed to complexionbetween ligand and Ag^+ causing the formation of separate AgNPs in ligand matrix. This result, in turn, isinduced by the activity of silver cation with OH and NO_2groups inligand and methanol solvent that can reduce the silver ion.

Analysis of Schiff base ligand

The other characterization techniques were analysed for the confirmation of formation of Schiff base such as ESI-Mass, ^{1}H-NMR and elemental composition and it was displayed in Fig. 7. It clearly proved as the M + 1 peak and chemical shifts of protons in Schiff base were well matched.

3.2. Proposed mechanism involved in the development of AgNPs

In this work, we have utilized Schiff base as a capping agent for the development of AgNPs. The structure of Schiff base which is involved in the formation of AgNPs is made up of imine group, which contains the carbonyl, nitro, and hydroxyl groups in abundance. The number of carbonyl and hydroxyl groups helps in the complexation of Ag^+ ions. These Ag^+ ions oxidize the hydroxyl to carbonyl groups, during which the Ag^+ ions are reduced to elemental Ag.

3.3. Catalytic degradation of dyes using the synthesized AgNPs

The synthesized Schiff base ligand capped AgNPs were employed for the catalytic degradation of environmentally persistent dyes such as MB, RhB, and EY dyes in the presence of $NaBH_4$ as a reducing agent (Fig. 8). The degradation of pure dye solution expressed no changes in absorption upon during the catalytic reaction without AgNPs and $NaBH_4$, while the test dye solution having AgNPs in all experiments expressed a gradual decrease in absorbance during the catalytic reaction in the presence of $NaBH_4$. Figure 8 shows that the rate of absorption bands of MB, RhB, and EY from UV–Vis spectrophotometer at 663 nm, 554 nm, and 534 nm due to n → π* transition of C = N, C = O groups. Wavelength for each decreased maxima was recorded and final overlays were formed upon the discolouration. UV–vis overlay spectra show this gradual absorbance reduction corresponds to the increase in degradation efficiency. AgNPs succeeded in degrading 71.58% of MB, 50.16% of RhB, and 80.99% of EY in 80 min with small amount of catalyst (10 µL). The order of degradation of dyes is EY > MB > RhB (Fig. 9). Figure 9 illustrates that the reaction kinetics (ln (A_0/A_t) vs time) for determining the apparent rate constant of catalytic

degradation reactions of dyes. For all the dyes, the degradation caused by AgNPs was found to be pseudo first-order kinetics. There was a linear relationship between ln (A_0/A_t) vs time with R^2 = 0.98, 0.97, and 0.98 for MB, RhB, and EY, respectively. The apparent rate constants were 0.248 min^{-1}, 0.186 min^{-1}, and 0.285 min^{-1} were observed for the degradation of MB, RhB, and EY dyes using AgNPs, respectively.

3.4. Sensing activity for the detection of Fe^{2+}

To test their analytical application as a fluorescent sensor, we studied their SPR properties and tendency to agglomerate in the presence of the analyte. The employability of AgNPs as an optical probe for harsh metal ions is significantly centered on the examination of variations in position and/or intensity of plasmon band and color of the nanoparticle solution. If the interaction of nanoparticles is selective towards only one metal ion, this may become the basis of metal detection [47–48]. Based on this observation, initially we inspected visually, the interaction of different metal ions (Pb^{2+}, Cd^{2+}, Co^{2+}, Fe^{2+}, K^{+}, Mg^{2+}, Ni^{2+}, Hg^{2+}, Sr^{2+}, Ca^{2+}, Ba^{2+}, Al^{3+} and Cr^{3+}) individually with AgNPs and later obtained the emission spectra of the assay solutions (Fig. 10). Out of these metal ions, only Fe^{2+} ion exhibited significant change the PL intensity in the emission spectra and the color of the solution, which can be easily observed with the naked eye. This indicates that AgNPs can be used as a fluorescent sensor to detect Fe^{2+} ion in an aqueous medium either without any modification or sample pre-treatment other than metal ions. Therefore, the selective interaction of AgNPs with Fe^{2+} ions over the other environmentally relevant heavy metal ions could be due to the presence of nitro ($-NO_2$) and hydroxyl (−OH) groups on the surface of AgNPs. It is noticed that only Fe^{2+} ion exhibited a substantial change in the spectrum with a red-shift of the λ_{max} from 472 to 485 nm with intensity decreasing and a sharp color change from yellow to orange, detectable by naked-eye. The shift in λ_{max} of the plasmon band and the color change of the solution is due to aggregation of AgNPs induced by Fe^{2+} ion through the coordination covalent bonding between the surface functional groups of Ag NPs and Fe^{2+} ion. However, there is a drastic change in the absorption spectra and color of AgNPs upon the addition of Fe^{2+} ion, confirming that the Schiff base consisting electron donors on the surfaces of AgNPs play key role to interact with Fe^{2+} via coordinate covalent bond, resulted in a red shift and a color change.

For practical applications, it is essential to establish the sensing response and minimum detection limit of the system. Therefore, to quantitatively establish the dynamic detection concentration of Fe^{2+} ions by AgNPs, several repeated experiments were carried with varying dilutions of Fe^{2+}. The concentration of the solution is increasing from 1 μM to 100 μM, the alteration in its intensity from higher to lower (Fig. 10). Furthermore, a large decline in intensity with distinct color changes was observed with increasing at the concentration of 100 μM. This interaction of Fe^{2+} ions leads to the disintegration of AgNPs that result in a decrease in the concentration of free scattered colloidal AgNPs. It was observed that this diluted colloidal AgNPs solution showed a lower limit of detection (LOD) = 0.284 μM (284 nM), which might be due to the reason that dilution results into excellent dispersal of AgNPs and addition of even very little amount of Fe^{2+} ions are enough for etching of available particles. Based on these investigations, it can

be clinched that more dilution of AgNPs solution may result in detection of mercury ions to further lower limit.

The Stern-Volmer constant (K_{SV}) of the Schiff base ligand and its capped AgNPs were determined by Stern-Volmer equation:

$I / I_0 = 1 + K_{sv} [Q]$

K_{SV} is the Stern-Volmer quenching constant, [Q] is the concentration of quencher (ligand, Ag NPS), I and I_0 are the presence and absence of quencher fluorescence intensities. K_{sv} of values of ligand and AgNPs are 3.62×10^4 and 2.87×10^5. The obtained K_{sv} of values of prepared compounds indicate that AgNPs has better sensing activity than ligand towards the detection of Fe^{2+} in nano-molar range of concentration.

3.5. Antimicrobial activity

Antimicrobial action of Schiff base capped AgNPs was tested against Gram-negative (*P. aeruginosa* and *E. coli*) and Gram-positive (*B. subtilis* and *S. aureus*) bacterial strains and results were shown in Fig. 11. The outcomes demonstrated that the synthesized AgNPs have discrete antibacterial action against pathogenic microorganisms at 5 µg/mL concentration. AgNPs were contrasted positively with silver nitrate, Schiff base and standard antibiotic, ampicillin at equal concentration [49]. The AgNPs revealed more bacterial growth inhibition action than silver nitrate and Schiff base. AgNPs were genuinely lethal to *S. aureus, B. subtilis*, and *E. coli* with inhibition zone of 17.4, 16.6, and 18.6 mm. The AgNPs indicated less antibacterial action against *E. coli, S. aureus* and *B. subtilis* and furthermore, high activity against *P. Aeruginosa* (20.8 mm) can be inferred that the blended AgNPs demonstrated noteworthy antibacterial activity on both gram classes of microorganisms [50]. The cell membraneof bacteria consists of proteins containing sulfur, and the AgNPs interact with these proteins as well as thephosphorus-containing compounds like DNA. Therefore, these AgNPs can cause structural changes in the bacterialcell wall and nuclear membrane ultimately leading to celldistortion and death [51]. For Schiff base capped AgNPs, the higher activity compared to the free ligand may berelated to chelation of the metal ion with donor atoms of the ligand [52] that reduces polarity of the metal ion. As aresult, an increase occurs in the lipophilic character, favouring the permeation through lipid layers of the bacterial membrane that damages the outer cell membrane and consequently inhibits the growth of bacteria [53].

In addition, the synthesized AgNPs were exhibited high antifungal activity, and this property can be very useful, especially against microorganisms resistant to conventional antimicrobials such as *A. niger* and *C. albicans* showed high sensitivity to AgNPs (Fig. 11). The antifungal activity results of 20 µg of AgNPs can be compared with the activity of ketoconazole as a standard antifungal. Among the tested fungi, *A. niger* had the most (12.1 mm) and *C. ablicans* (10.5 mm) had the least sensitive fungus detected by using the synthesized Schiff base and AgNPs. The percentage of growth inhibition due to the effect of AgNPs was analyzed by statistical software SAS. Results confirmed a significant effect of AgNPs on fungal growth inhibition at 1% confidence interval.

3.6. Mechanism of antimicrobial activity of Ag NPs

The mechanism of antimicrobial activity of metal nanoparticles such as AgNPs has been testified by numerous researchers, the cell death and leakage of cell membrane is because of the discharge of Ag^+ ion and generation of reactive oxygen species (singlet oxygen, superoxide anion radical, hydroxyl radical and hydrogen peroxide) the smaller size particles gives a more reactive surface zone to interact with the bacteria enhancing a superior anti-bacterial ability. The production ofthe reactive oxygen specieson the surface of the AgNPs, when the light causes oxidative stress in the bacterial cell wall, eventually it leads to the death of the cells [54]. Ag with a positive charge and cell membrane with negative charge mutually attract. Further, Ag^+ enters into the cell membrane and reacts with the thiol groups present on the cell membrane and destruction it leading to the death of the cells.

3.7. Antioxidant activity

In the present study, the antioxidant activity of the synthesized Schiff bas capped AgNPs was studied by using DPPH method. The antioxidant activity of synthesized AgNPs was assessed in terms of percentage inhibition of DPPH radicals in the presence of ascorbic acid. The DPPH is considered more stable nitrogen-cantered free radical due to exhibiting a higher degree of accepting hydrogen atoms or electrons from antioxidant materials [55]. The DPPH solution color change was observed on the addition of AgNPs, which is due to the scavenging action of DPPH by addition of hydrogen to form the yellow-colored DPPH. The scavenging ability was quantified using spectrophotometer by taking optical density at 517 nm. The percentage of antioxidant activity of Schiff base and AgNPs were calculated and compared with Schiff base. The resultsare clearly indicated as AgNPs exhibited high DPPH activity (68.24%) than the Schiff base (44.86%), moreover the standard compound (ascorbic acid) shown maximum DPPH activity (86.38%) and the results were illustrated in Fig. 12. However, the AgNPs showed very good or almost equivalent free radical scavenging activity. The free radical scavenging activity of synthesized AgNPs might be due the active components present on the surface of the nanoparticles and they were ready to give up hydrogen atom from their hydroxyl groups to free radicals and form stable phenoxy radicals.

4. Conclusions

In this summary, we have synthesized 2-[(4-methoxy-phenyl)iminomethyl]-4-nitrophenolas Schiff base derived from p-anisidine and 5-nitrosalicylaldehyde and Schiff base capped AgNPs. The formation of the Schiff base and AgNPs were analyzed using UV–vis spectrophotometer, PL, FTIR, XRD, SEM, and TEM. The powder XRD pattern shows that the synthesized AgNPs is cubic phase structure with an average crystallite size (D) is 10 ± 2 nm and band gap value is 2.88 eV, which is calculated from UV-vis absorption spectrum. TEM image confirms the formation of AgNPs with almost spherical in shape. Theses nanoparticles show more stability and virtuous catalytic activity toward the degradation of MB, RhB and EY in the presence of $NaBH_4$ as a reducing agent. The PL band in the visible range resulting from the higher surface interstitial defects reduces the electrons/holes recombination and consequently increases the catalytic activity. Finally, the synthesized AgNPs exhibited a significant bactericidal and fungal

activity against *S. aureus, E. coli, B. Subtilis*and *P. aeruginosa*; *A. niger* and *C. ablicans* using the disc diffusion method. AgNPs revealed that they had good antimicrobial activity and they also had effective free radical scavenging efficacy by DPPH method. Finally, it was concluded that the synthesized Schiff base ligand capped AgNPs showed better catalytic, sensing, and biological results, so it has proved to exhibit excellent multifunctional biomedical applications in future.

Declarations

Acknowledgments The authors wish to thank the Head, University of College of Saifabad, Osmania University, Hyderabad and Telangana University, Nizamabad, Telangana State for the excellent support toward research.

Author Declarations

1. Authors' contributions All authors contributed to the study conception and design. Material preparation, data collection and analysis were performed by G. Suneetha. The first draft of the manuscript was written by P.S. Manjari. All authors read and approved the final manuscript.

2. Conflicts of interest/Competing interests The authors declare they have no competing interests.

3. Funding No funding was received for this study.

4. Ethics Declaration statement Not applicable as the study does not include any use of animals and humans.

5. Consent to Participate Not applicable

6. Consent for publication Not applicable

7. Availability of data and material/ Data availability Not applicable

References

1. H. Unver, Z. Hayvali, Synthesis, spectroscopic studies and structures of square-olanar nickel(II) and copper(II) complexes derived from 1-{(z)-[furan-2-ylmethyl]imino]methyl}-6-methoxy phenol, Spectrochim Acta A. 75 (2010) 782–788.
2. S. Kaya, S. Erkan, D. Karakaş, Computational investigation of molecular structures, spectroscopic properties and antitumor-antibacterial activities of some Schiff bases. Spectrochim. Acta Part A: Mol. Biomol. Spectroscopy 244 (2021) 118829.
3. Y. Xie, L. Yan, Y. Tang, M. Tang, S. Wang, L. Bi, W. Sun, J. Li, A smart fluorescent probe based on salicylaldehyde schiff's base with AIE and ESIPT characteristics for the detections of N2H4 and ClO−, J. Fluoresce. 29 (2019) 399-406.

4. Y. Song, Z. Xu, Q. Sun, B. Su, Q. Gao, H. Liu, J. Zhao, Synthesis, structures, characterization of copper(II), nickel(II), and cobalt(III) metal complexes derived from an asymmetric bidentate Schiff base ligand, J.Coord. Chem. 61 (2008) 1212–1220.
5. S. Mandal, A.K. Rout, G. Pilet, D. Bandyopadhyay, Synthesis, crystal structure and characterization of two new copper(II) complexes of Schiff bases derived from furfurylamine, Trans. Met. Chem. 34 (2009) 719–724.
6. S.P. Xu, P.C. Lv, R.Q. Fang, L. Shi, H.L. Zhu, Synthesis and crystal structure of 2,4-diiodo-6-[(2-morpholin-4-yl-ethylimino)-methyl]-phenolato-zinc(II), J. Chem.Crystallogr. 39 (2009) 931–934.
7. E. Ispir, The synthesis, characterization, electrochemical character, catalytic and antimicrobial activity of novel azo containing Schiff bases and their metal complexes, Dyes Pigm. 82 (2009) 13–19.
8. T. Akitsu, Y. Einaga, Synthesis, crystal structures and electronic properties of Schiff base nickel(II) complexes: towards solvatochromism induced by a photochromic solute, Polyhedron 24 (2005) 1869–1877.
9. G. Avsar, H. Altinel, M.K. Yilmaz, B. Guzel, Synthesis, characterization, and thermal decomposition of fluorinated salicylaldehyde Schiff base derivatives (salen) and their complexes with copper(II), J. Therm. Anal.Calorim. 101 (2010) 199–203.
10. S. Oz, M. Kunduraci, R. Kurtaran, U. Ergum, C. Arici, M.A. Akay, O. Atakol, K.C. Emregul, D. Ulku, Thermal decomposition of linear tetranuclear copper(II) complexes including l-azido bridges, J. Therm. Anal.Calorim. 101 (2010) 221–227.
11. D.Ayodhya, G.Veerabhadram, Fabrication of Schiff base coordinated ZnS nanoparticles for enhanced photocatalytic degradation of chlorpyrifos pesticide and detection of heavy metal ions, J.Materiomics 5 (2019) 446–454.
12. I. Sk, M.A. Khan, A. Haque, S. Ghosh, D. Roy, S. Homechuadhuri, M.A. Alam,Synthesis of gold and silver nanoparticles using Malvaverticillata leaves extract: Study of gold nanoparticles catalysed reduction of nitro-Schiff bases and antibacterial activities of silver nanoparticles, Current Res. Green Sust. Chem. 3 (2020)100006.
13. M.A. Halcrow, Christou G. Biomimetic chemistry of nickel, Chem. Rev. 94 (1994) 2421–2481.
14. M. Azharuddin, G.H. Zhu, D. Das, E. Ozgur, L. Uzun, A.P.F. Turner, H.K. Patra, A repertoire of biomedical applications of noble metal nanoparticles, Chem. Commun.55(2019)6964–6996.
15. G. Gahlawat, A.R. Choudhury, A review on the biosynthesis of metal and metal salt nanoparticles by microbes, RSC Adv. 9(2019) 12944–12967.
16. J.J. Erbs, B. Gilbert, R.L. Penn, Influence of size on reductive dissolution of six-line Ferrihydrite, J. Phys. Chem. C 112(2008) 12127–12133.
17. J.G. Hinman, J.R. Eller, W. Lin, J. Li, J. Li,C.J. Murphy, Oxidation state of capping agent affects spatial reactivity on gold nanorods, J. Am. Chem. Soc. 139(2017)9851–9854.
18. A. Sedighi, M. Montazer,Tunable shaped N-doped CuO nanoparticles on cotton fabric through processing conditions: synthesis, antibacterial behavior and mechanical properties, Cellulose 23(2016)2229–2243.

19. P.C. Lee, D. Meisel, Adsorption and surface-enhanced Raman of dyes on silver and gold sols, J. Phys. Chem. 86(1982)3391–3395.
20. L. Longenberger, G. Mills, Formation of metal particles in aqueous solutions by reactions of metal complexes with polymers, J. Phys. Chem. 99(1995)475–478.
21. S.D. Bunge, T.J. Boyle, T.J. Headley, Synthesis of coinagemetal nanoparticles from mesityl precursors, Nano Lett. 3(2003)901–905.
22. M. Brust, M. Walker, D. Bethell, D.J. Schiffrin, R. Whyman, Synthesis of thiol-derivatised gold nanoparticles in a two-phase liquid–liquid system, J. Chem. Soc. Chem. Commun. 7 (1994) 801–802.
23. L.M. Rossi, J.L. Fiorio, M.A.S. Garcia, C.P. Ferraz, The role and fate of capping ligands in colloidally prepared metal nanoparticle catalysts, Dalton Trans. 47(2018)5889–5915.
24. J.D.S. Newman, G.J. Blanchard, Formation of gold nanoparticles using amine reducing agents, Langmuir 22 (2006)5882–5887.
25. C. Battocchio, C. Meneghini, I. Fratoddi, I. Venditti, M.V. Russo, G. Aquilanti, C.M.F. Bondino, R.M.M. Rossi, S.M. Giovanni, Silver nanoparticles stabilized with Thiols: a close look at the local chemistry and chemical structure, J. Phys. Chem. C 116 (2012) 19571– 19578.
26. F. Kretschmer, U. Mansfeld, S. Hoeppener, M.D. Hager, U.S. Schubert,Tunable synthesis of poly(ethylene imine)-gold nanoparticle clusters, Chem.Commun. 50 (2014) 88–90.
27. Y. Tauran, A. Brioude, A.W. Coleman, M. Rhimi, B. Kim, Molecular recognition by gold, silver and copper nanoparticles, World J. Biol. Chem. 4 (2013)35–63.
28. K. Aslan, J. Zhang, J.R. Lakowicz, C.D. Geddes, Saccharide sensing using gold and silver nanoparticles-a review, J. Fluoresce. 14 (2004) 391-400.
29. Y.Y. Loo, Y. Rukayadi, M.A. Nor-Khaizura, C.H. Kuan, B.W. Chieng, M. Nishibuchi, S. Radu, In vitro antimicrobial activity of green synthesized silver nanoparticles against selected gram-negative foodborne pathogens, Front. Microbiology 9 (2018) 1555.
30. G. Lakshmanan, A. Sathiyaseelan, P.T. Kalaichelvan, K. Murugesan, K. Plant-mediated synthesis of silver nanoparticles using fruit extract of Cleome viscosa L.: Assessment of their antibacterial and anticancer activity. Karbala Int. J. Mod. Sci. 4, 61–68 (2018).
31. M.I. Skiba, V.I. Vorobyova, I.V. Kosogina, Preparation of silver nanoparticles in a plasma-liquid system in the presence of PVA: Antimicrobial, catalytic, and sensing properties, J. Chem. 2020(2020) 5380950.
32. D. Ayodhya, M. Venkatesham, A.S. Kumari, G.B. Reddy, D. Ramakrishna, G. Veerabhadram, Synthesis, characterization, fluorescence, photocatalytic and antibacterial activity of CdS nanoparticles using Schiff base, J. Fluorescence 25 (2015) 1481-1492.
33. E.S. Azam, W.A. El-Said, Synthesis of copper/nickel nanoparticles using newly synthesized Schiff-base metals complexes and their cytotoxicity/catalytic activities, Bioorg. Chem. 57 (2014) 5-12.

34. S. Raj, H. Singh, R. Trivedi, V. Soni, Biogenic synthesis of AgNPs employing Terminalia arjuna leaf extract and its efficacy towards catalytic degradation of organic dyes, Sci. Reports 10 (2020) 1-10.
35. B. Janani, A. Syed, L.L. Raju, N. Marraiki, A.M. Elgorban, N.S. Zaghloul, A.M. Thomas, A. Das, S.S. Khan, Highly selective and effective environmental mercuric ion detection method based on starch modified Ag NPs in presence of glycine, Optics Commun. 465 (2020) 125564.
36. P. Adwin Jose, J. Dhaveethu Raja, M. Sankarganesh, J. Rajesh, Evaluation of antioxidant, DNA targeting, antimicrobial and cytotoxic studies of imine capped copper and nickel nanoparticles, J. Photochem. Photobiol. B 178 (2018) 143–151.
37. D. Ayodhya, G. Veerabhadram, Highly efficient sunlight-driven photocatalytic degradation of organic pollutants and fluorescence detection of Hg^{2+} using multifunctional GO-Bi_2S_3 nanostructures, J. Photochem. Photobiol. A: Chem. 356 (2018) 545-555.
38. S. Tawata, S. Taira, N. Kobamoto,J. Zhu, M. Ishihara, S. Toyama, Synthesis and antifungal activity of cinnamic acid esters. Bioscience, biotechnology, and biochemistry, 60 (1996) 909-910.
39. D. Ayodhya, G. Veerabhadram, Green synthesis of garlic extract stabilized Ag@CeO_2 composites for photocatalytic and sonocatalytic degradation of mixed dyes and antimicrobial studies, J. Mol. Struct.1205 (2020) 127611.
40. M. Ghasemian, A. Kakanejadifard, T. Karami, Synthesis, structural characterization, antimicrobial activities and theoretical investigations of some 4-(4-aminophenylsulfonyl) phenylimino) methyl)-4-(aryldiazenyl) phenol,Spectrochim.Acta Part A: Molecular and Biomolecular Spectroscopy 168 (2016) 190-198.
41. M. Sahu, P. Biswas, Single-step processing of copper-doped titania nanomaterials in a flame aerosol reactor, Nanoscale Res.Lett.6 (2011) 1-14.
42. N. Raman, S. Sudharsan, Phase transfer synthesis of N,N'(1,2-phenylene)bis-hippuricamide tethered metal based functionalized nanoparticles: A study on some novel microbial targeting peptidemimic nanoparticles, Appl. Surf. Sci. 257(2011)10659–10666.
43. T. Fukaminato, T. Sasaki, T. Kawai, N. Tamai, M. Irie, Digital photoswitching of fluorescence based on the photochromism of diarylethene derivatives at a single-molecule level, J. Am. Chem. Soc. 126 (2004) 14843-14849.
44. R.M. Silverstein, G.C. Bassler, T.C. Morrill, Spectrometric identification of organic compounds, 4th, New York, NY, USA, 1981.
45. D. Nayak, S. Ashe, P.R. Rauta, M. Kumari, B. Nayak, Bark extract mediated green synthesis of silver nanoparticles: evaluation of antimicrobial activity and antiproliferative response against osteosarcoma, Mater. Sci. Eng: C 58(2016) 44–52.
46. T. Jiao, H. Guo, Q. Zhang, Q. Peng, Y. Tang, X. Yan, B. Li, Reduced graphene oxide-based silver nanoparticle-containing composite hydrogel as highly efficient dye catalysts for wastewater treatment, Sci. Rep. 5(2015) 1-12.

47. D. Ayodhya, G. Veerabhadram, Green synthesis, characterization, photocatalytic, fluorescence and antimicrobial activities of Cochlospermumgossypium capped Ag_2S nanoparticles, J. Photochem. Photobiol. B 157 (2016) 57-69.
48. D. Ayodhya, G. Veerabhadram, Preparation, characterization, photocatalytic, sensing and antimicrobial studies of Calotropisgigantea leaf extract capped CuS NPs by a green approach, J. Inorg. Organomet. Poly. Mater. 27 (2017) 215-230.
49. A.B. Hanan, A.M. Abdel-Mohsen, E.E. Hossam, Green-assisted tool for nanogold synthesis based on alginate as a biological macromolecule, RSC Adv. 6 (2016) 73974–73985.
50. A.D.J. Ruíz-Baltazar, S.Y. Reyes-López, D. Larrañaga, M. Estévez, Green synthesis of silver nanoparticles using a Melissa officinalis leaf extract with antibacterial properties, Results Phys. 7 (2017) 2639–2643.
51. H.Y. Song, K.K. Ko, L.H. Oh, B.T. Lee, Fabrication of silver nanoparticles and their antimicrobial mechanisms, Eur. Cells Mater. 11 (2006) 58.
52. P.K. Stoimenov, R.L. Klinger, G.L. Marchin, K.J. Klabunde, Metal oxide nanoparticles as bactericidal agents, Langmuir 18 (2002) 6679-6686.
53. A.A. Osowole, G.A. Kolawole, O.E. Fagade, Synthesis, characterization and biological studies on unsymmetrical Schiff-base complexes of nickel (II), copper (II) and zinc (II) and adducts with 2,2'-dipyridine and 1,10-phenanthroline, J.Coord. Chem. 61 (2008) 1046-1055.
54. D. Ayodhya, G. Veerabhadram, Facile thermal fabrication of CuO nanoparticles from Cu(II)-Schiff base complexes and its catalytic reduction of 4-nitrophenol, antioxidant, and antimicrobial studies, Chem. Data Collections23 (2019) 100259.
55. Y.K. Mohanta, S.K. Panda, R. Jayabalan, N. Sharma, Antimicrobial, antioxidant and cytotoxic activity of silver nanoparticles synthesized by leaf extract of Erythrinasuberosa (Roxb.), Front. Mol. Biosci. 4 (2017) 1–9.

Figures

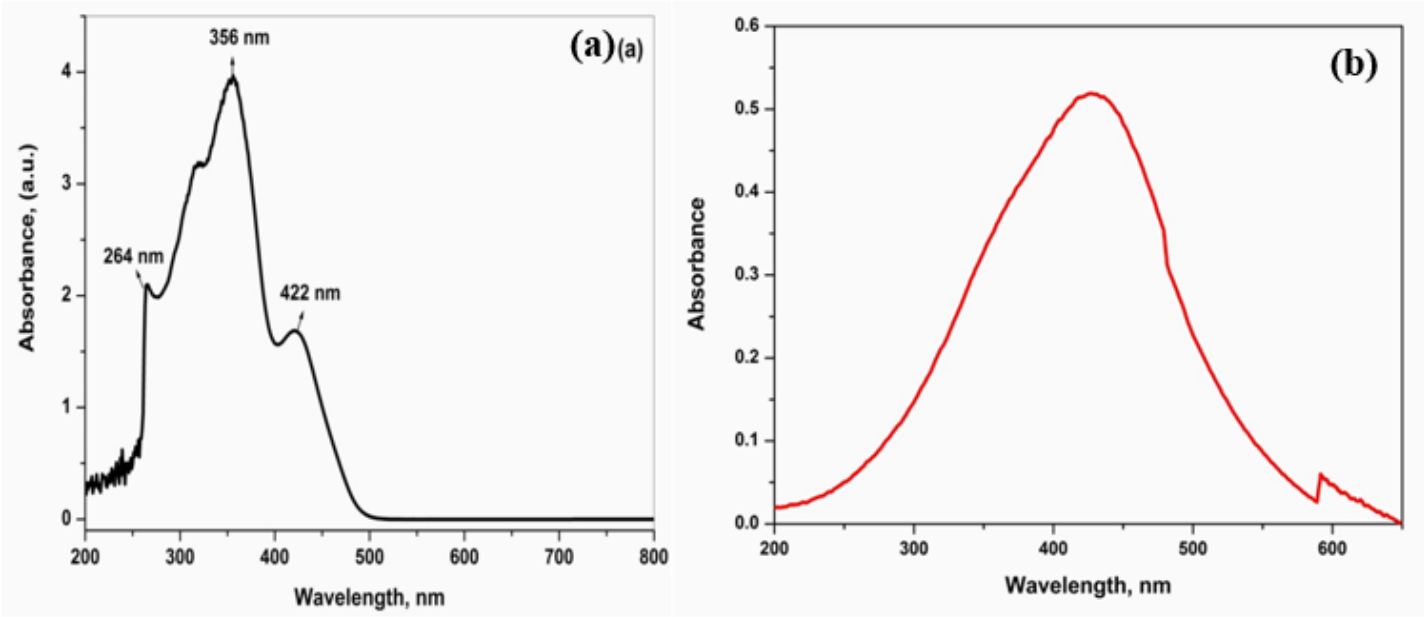

Figure 1

UV-visible absorption spectra of (a) Schiff base and (b) Schiff base ligand capped AgNPs

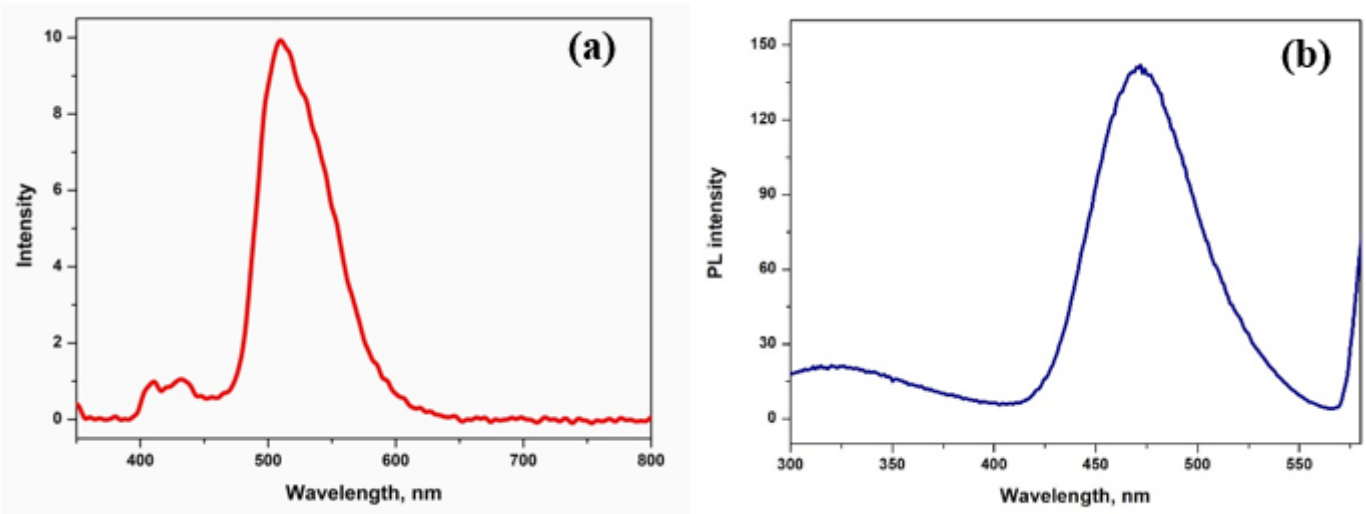

Figure 2

PL spectra of (a) Schiff base and (b) Schiff base ligand capped AgNPs

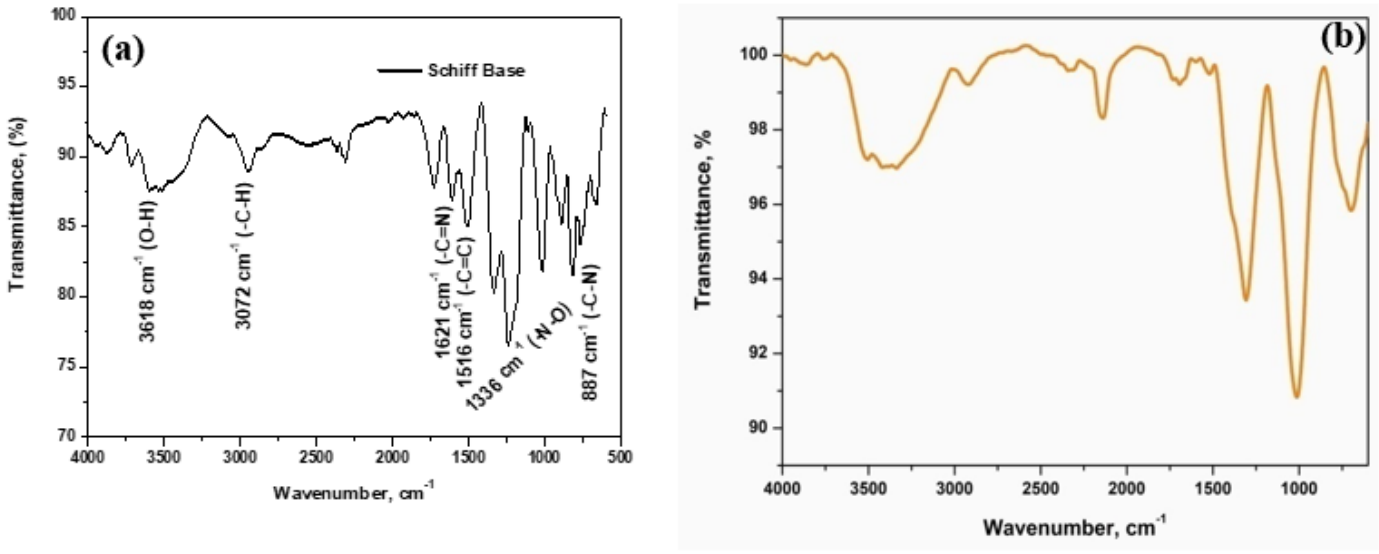

Figure 3

FTIR spectra of (a) Schiff base and (b) Schiff base ligand capped AgNPs

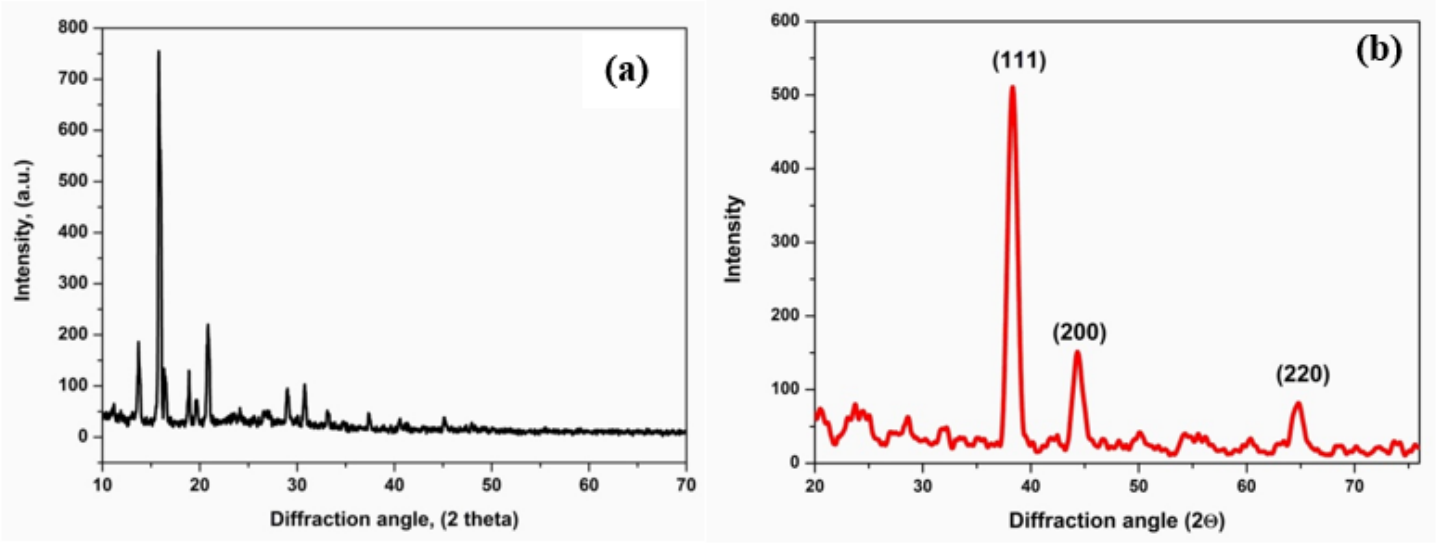

Figure 4

Powder XRD spectra of (a) Schiff base and (b) Schiff base ligand capped AgNPs

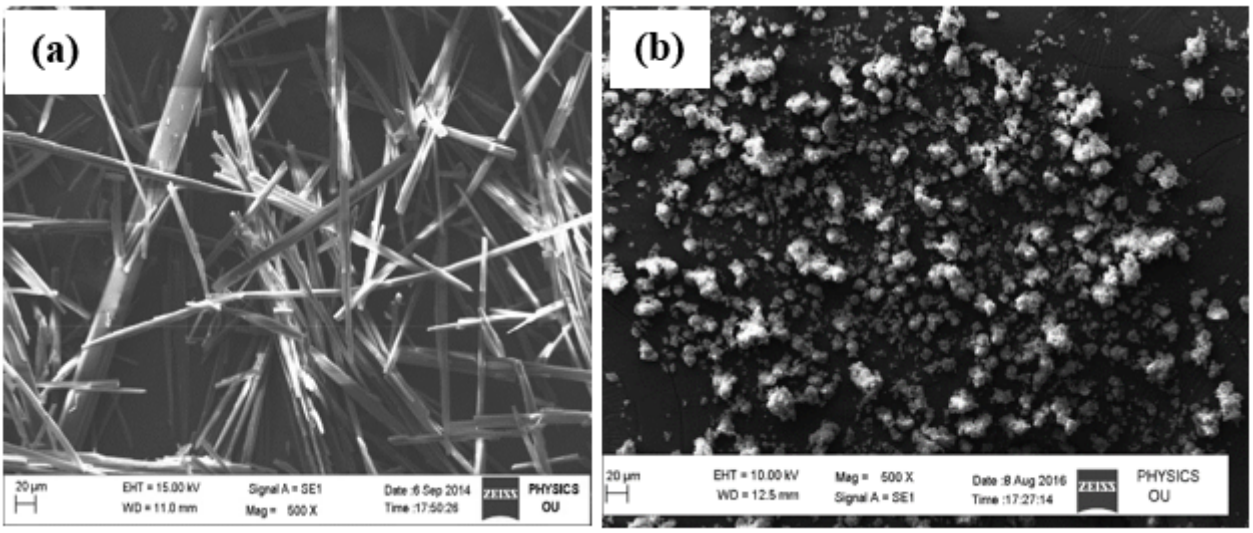

Figure 5

SEM images of (a) Schiff base and (b) Schiff base ligand capped AgNPs

Figure 6

TEM image of the Schiff base ligand capped AgNPs

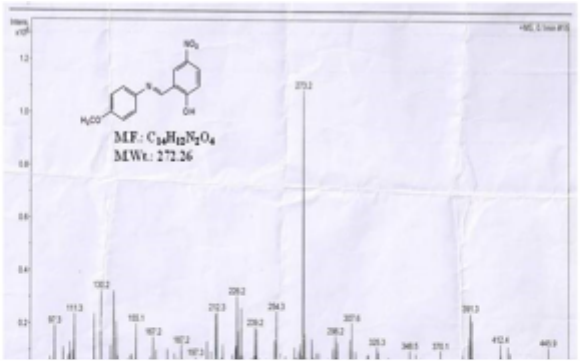

Figure 7

ESI-Mass,^{1}H-NMR and EDAX spectra of synthesized Schiff Base

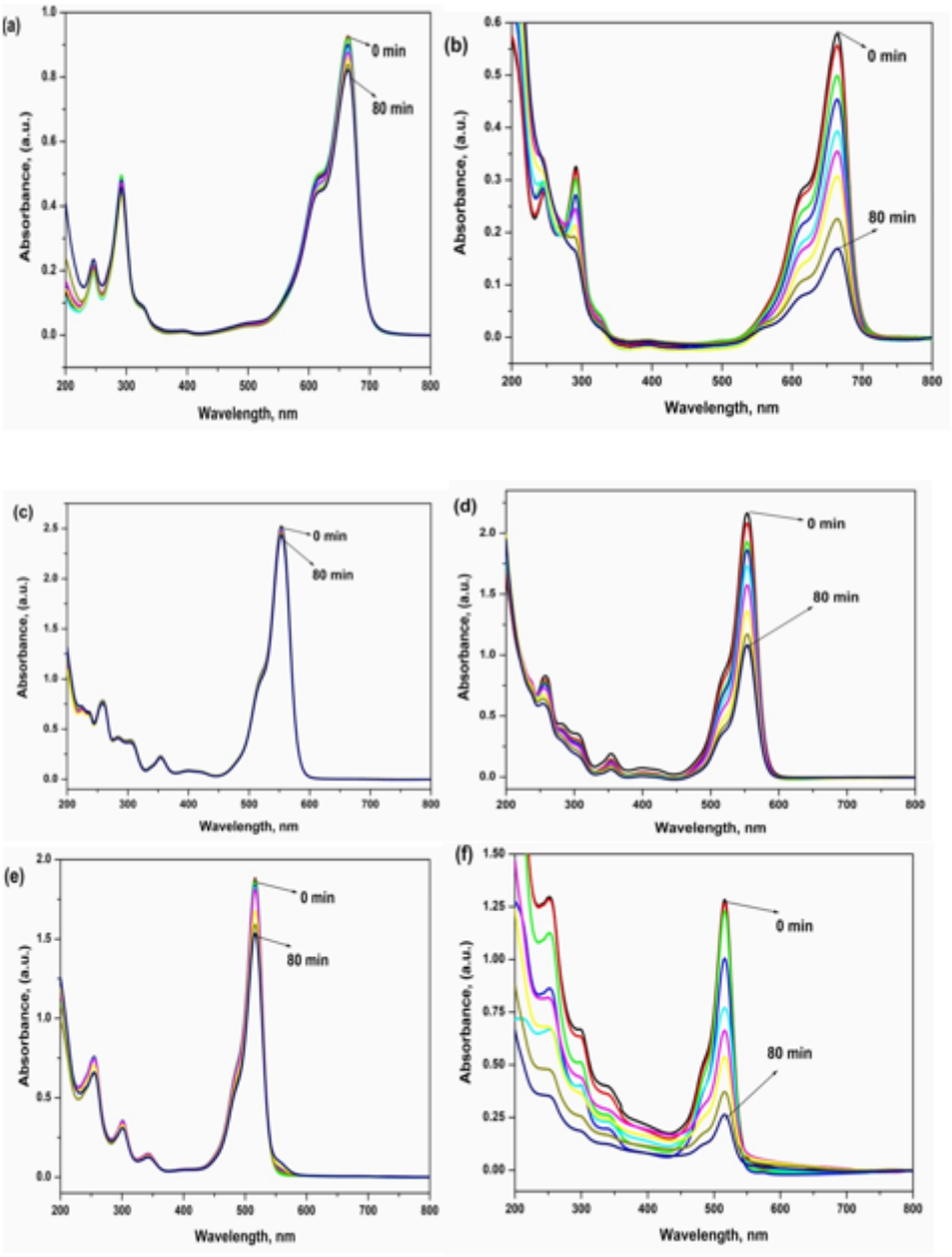

Figure 8

The UV-vis absorption degradation spectra of (a-b) MB, (c-d) RhB, and (e-f) EY dyes using absence and presence of AgNPs and $NaBH_4$, respectively

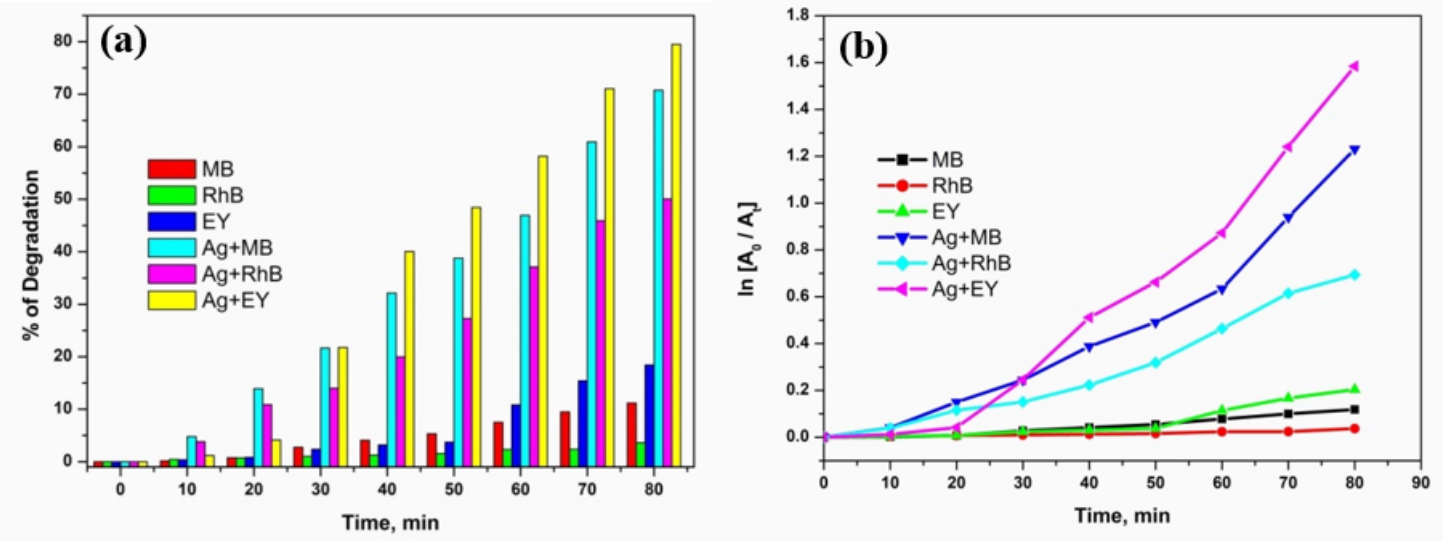

Figure 9

(a) The degradation efficiency and (b) kinetics plots for the catalytic degradation of MB, RhB, and EY dyes using AgNPs

Figure 10

(a) PL spectra of AgNPs upon the addition of various metal ions (K^+, Ba^{2+}, Cd^{2+}, Fe^{2+}, Sr^{2+}, Mg^{2+}, Co^{2+}, Pb^{2+}, Ni^{2+}, Ca^{2+}, Hg^{2+}, Al^{3+},and Cr^{3+}, 0.1 μM) along without and with the addition of Fe^{2+}ion;(b) PL spectra of AgNPs upon the addition of Fe^{2+} ion concentration in the range of 0.1-100 μM and (c) Stern-Volmer plot

Figure 11

(a) Antibacterial and (b) antifungal activities of the synthesized Schiff base and AgNPs

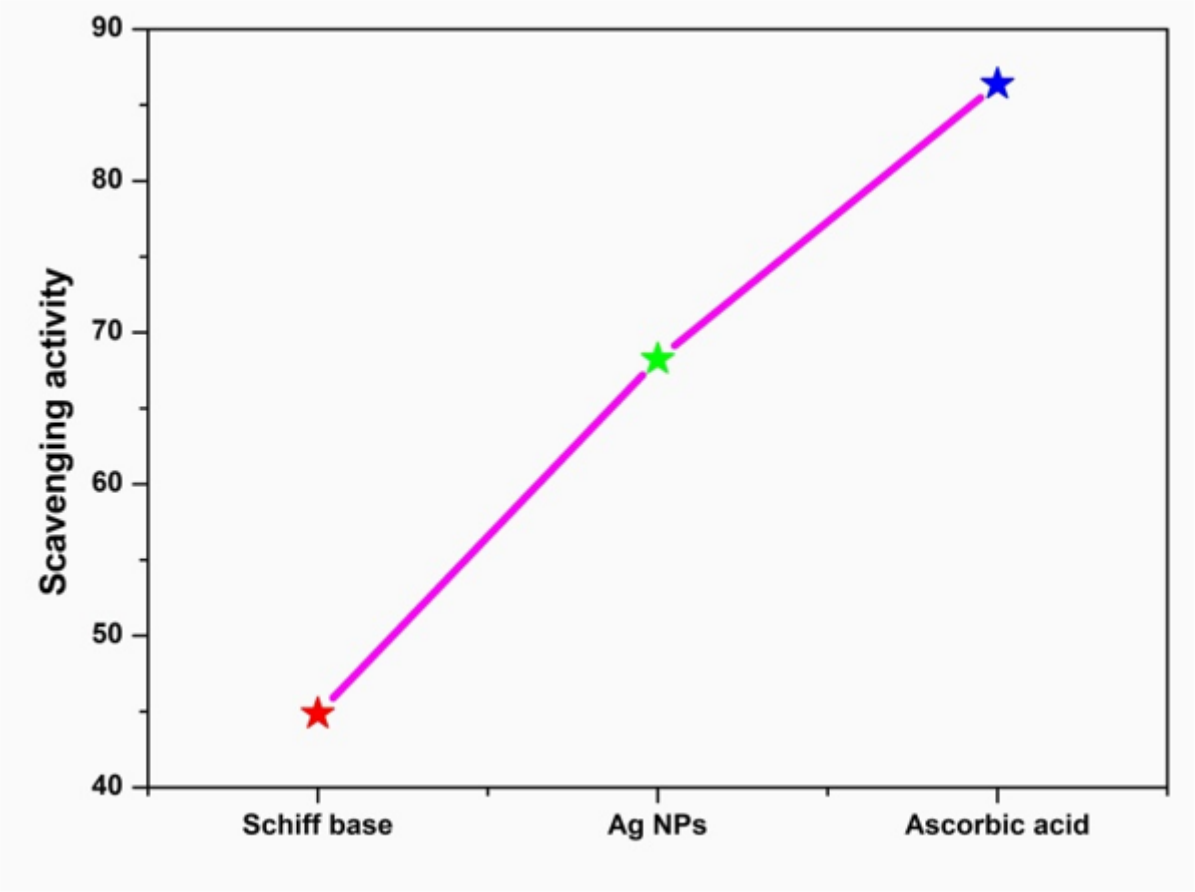

Figure 12

The antioxidant activity of the synthesized Schiff base and AgNPs with standard ascorbic acid

Supplementary Files

This is a list of supplementary files associated with this preprint. Click to download.

- GA.png
- Scheme1.png
- Scheme2.png